OPEN ACCESS Freely available online

PLOS ONE

CO_2-Driven Ocean Acidification Alters and Weakens Integrity of the Calcareous Tubes Produced by the Serpulid Tubeworm, *Hydroides elegans*

Vera Bin San Chan[1], Chaoyi Li[1], Ackley Charles Lane[1], Yanchun Wang[2], Xingwen Lu[2], Kaimin Shih[2], Tong Zhang[2], Vengatesen Thiyagarajan[1]*

1 The Swire Institute of Marine Science and School of Biological Sciences, The University of Hong Kong, Pokfulam, Hong Kong, Special Administrative Region, People's Republic of China, **2** Department of Civil Engineering, The University of Hong Kong, Pokfulam, Hong Kong, Special Administrative Region, People's Republic of China

Abstract

As a consequence of anthropogenic CO_2-driven ocean acidification (OA), coastal waters are becoming increasingly challenging for calcifiers due to reductions in saturation states of calcium carbonate ($CaCO_3$) minerals. The response of calcification rate is one of the most frequently investigated symptoms of OA. However, OA may also result in poor quality calcareous products through impaired calcification processes despite there being no observed change in calcification rate. The mineralogy and ultrastructure of the calcareous products under OA conditions may be altered, resulting in changes to the mechanical properties of calcified structures. Here, the warm water biofouling tubeworm, *Hydroides elegans*, was reared from larva to early juvenile stage at the aragonite saturation state (Ω_A) for the current pCO_2 level (ambient) and those predicted for the years 2050, 2100 and 2300. Composition, ultrastructure and mechanical strength of the calcareous tubes produced by those early juvenile tubeworms were examined using X-ray diffraction (XRD), Fourier transform infrared spectroscopy (FT-IR), scanning electron microscopy (SEM) and nanoindentation. Juvenile tubes were composed primarily of the highly soluble $CaCO_3$ mineral form, aragonite. Tubes produced in seawater with aragonite saturation states near or below one had significantly higher proportions of the crystalline precursor, amorphous calcium carbonate (ACC) and the calcite/aragonite ratio dramatically increased. These alterations in tube mineralogy resulted in a holistic deterioration of the tube hardness and elasticity. Thus, in conditions where Ω_A is near or below one, the aragonite-producing juvenile tubeworms may no longer be able to maintain the integrity of their calcification products, and may result in reduced survivorship due to the weakened tube protection.

Citation: Chan VBS, Li C, Lane AC, Wang Y, Lu X, et al. (2012) CO_2-Driven Ocean Acidification Alters and Weakens Integrity of the Calcareous Tubes Produced by the Serpulid Tubeworm, *Hydroides elegans*. PLoS ONE 7(8): e42718. doi:10.1371/journal.pone.0042718

Editor: Senjie Lin, University of Connecticut, United States of America

Received March 21, 2012; **Accepted** July 10, 2012; **Published** August 13, 2012

Funding: This study was supported by a research grant from the Research Grants Council, Hong Kong (no. 778309M). The funders had no role in study design, data collection and analysis, decision to publish, or preparation of the manuscript.

Competing Interests: The authors have declared that no competing interests exist.

* E-mail: rajan@hku.hk

Introduction

As a consequence of anthropogenic carbon dioxide (CO_2) emissions, the atmospheric CO_2 level has been increasing in an unprecedented rate. One third of this CO_2 is absorbed by the oceans through the process called "ocean acidification" (OA) [1]. This excess CO_2 decreases the pH, the carbonate ion (CO_3^{2-}) concentration and the calcium carbonate ($CaCO_3$) saturation states (Ω) in seawater [2]. The Arctic and Southern Oceans are expected to experience aragonite undersaturation before the middle of this century [3]. Similarly, estuaries and coastal waters may experience OA-like conditions sooner than the open ocean because of (a) anthropogenic addition of nutrients and eutrophication which consequently increases CO_2 concentrations and lowers pH [4,5], and (b) their inherently weak carbonate buffering capacity [6]. Therefore, top priority should be given to the study of biocalcification in benthic invertebrates and the challenges as in these naturally susceptible and variable coastal habitats [7].

The majority of benthic organisms living in coastal waters have complex life cycle, during which the pelagic larva must select a substrate, attach to it and then metamorphose into a benthic adult. This irreversible pelagic-benthic larval transition is an energetically expensive, delicate, and rapid process [8]. In calcifiers, these newly metamorphosed individuals must build a tough protective calcareous structure as soon as possible using a costly and complex biomineralization process [9,10]. In most larval forms, the formation of calcified structures starts from an unstable amorphous transient precursor of the calcitic or aragonitic forms of calcium carbonate defined by its irregular lattice structure, called amorphous calcium carbonate (ACC) [11,12]. ACC is subsequently transformed into the more stable forms of $CaCO_3$, aragonite and/or calcite [13–16]. Since aragonite is 35% more soluble than calcite [17], aragonite-producing organisms are expected to be especially vulnerable to CO_2-driven OA [18].

The ultrastructure and mechanical properties of calcareous structures produced under OA conditions, especially during the vulnerable early juvenile stage, may be compromised resulting in reduced survival [19–23]. There are several plausible mechanisms by which biomineralization under OA conditions could be affected. In order to cope with OA, organisms might differentially

allocate energy, favoring physiological homeostasis over the fabrication of calcareous tubes/skeltons/shells [24,25]. This change in energy allocation may favor the less costly, but more brittle, calcite polymorph of calcium carbonate. Calcite has lower organic content and a lower packing density of calcium and carbonate ions than aragonite [26]. Additionally, calcifiers experiencing OA stress may not have sufficient energy to construct the matrix proteins which are responsible for enhancing mechanical strength [27]. Secreting matrix proteins, such as the phosphate containing proteins known to stabilize ACC, is a vital process in shell production from the very initial stages often begun during the sensitve pelagic larval phase [28]. Finally, changes in ultrastructure and mechanical strength may be due to the preferential dissolution of more soluble polymorph of calcium carbonate, aragonite. Calcification under OA conditions may result in weaker products, e.g. partial loss of aragonite and/or production of disordered crystal morphologies might result in more brittle calcified structures dominated by poorly ordered calcite crystals. Regardless of the source(s) of alterations to calcium carbonate structures, any difference in the ability to produce orderly layered biominerals may also reduce the effectiveness of shells to protect against external attacks by predators like fishes and crabs [29,30]. The ability to calcify with structural and mechanical integrity is, therefore, an important focal point when evaluating the calcification responses of marine calcifiers to OA [20,31].

Among calcifying coastal organisms, the serpulid tubeworm (*Hydroides elegans*) is a commercially important fouling species whose calcification appears to be highly altered by OA [32]. Due to their unique larval metamorphosis pattern, rapid calcification immediately after metamorphosis, short generation time (3 to 4 weeks) and ease of culture in the laboratory, this species has long served as a model for larval biology and biofouling research [33]. Here, this species also provided a unique opportunity for us to examine their juvenile tube (shell) composition, structural integrity and mechanical strength as a function of increasing OA stress. This study sought to determine how OA will alter the composition and structure of the juvenile tube, and to what degree those alterations would affect its mechanical properties such as hardness and elasticity. This comparative analysis of calcareous tubes produced in ambient and OA environments by juvenile tubeworms is a very important first step toward understanding the interaction between biomineral production and the environment, which would ultimately, enabled us to better assess and predict the impact of OA on one of this commercially important calcifier.

Methods

Study organism

The calcareous tube forming (tubeworm), *Hydroides elegans* (Haswell, 1883), is a major polychaete species in coastal and estuarine biofouling communities [33]. This cosmopolitan warm water species completes its life-cycle in 3 to 4 weeks [34]. Adults of the tubeworm were collected during their peak reproductive season (January–March, 2011;16–17°C, salinity 30–32 ppt, and pH 8.0 to 8.2) from the floating structures in fish farms located at Yung Shue O, Hong Kong (22°27′N, 114°23′W). Animals were acclimatized in the laboratory for 3 to 7 days in an ambient temperature, pH and salinity condition. The female and male gonads were obtained from >30 randomly selected individuals and mixed to produce one, genetically diverse monoculture [35]. The majority of embryos developed into trochophore larvae within 12 h at 21°C, 33 ppt (salinity) and pH 8.1 [34]. This batch of newly hatched larvae was used for the following CO_2 perturbation experiment.

Design of the CO_2 perturbation experiment

Experimental design and CO_2 perturbation methodology suggested in the Guide for Best Practices in Ocean Acidification Research (http://www.epoca-project.eu) manual were used in this study to examine the effect of high partial pressure of CO_2 (pCO_2) or low pH (hereafter referred to as "low pH, high pCO_2" or OA treatments) on calcareous tubes built by the juvenile tubeworm [36]. There were three high pCO_2 treatments namely pCO_2~850 µatm (pH~7.9 and Ω_A~2), pCO_2~2000 µatm (pH 7.6 or Ω_A~1) and pCO_2~3000 µatm (pH 7.4 or Ω_A~0.7). The control treatment had the ambient pCO_2~500 µatm (pH 8.1 or Ω_A~3). The three high pCO_2 treatment levels were chosen to represent the pCO_2 level predicted by the "business-as-usual" emission scenario for the year 2050, 2100 and 2300, respectively [37]. The selected pCO_2 levels are also commonly observed in the natural carbonate system variability found in the subtropical estuarine and coastal waters where *H. elegans* is found [6,38,39].

The high pCO_2 levels were achieved by enriching ambient air with pure CO_2 using dual (air and CO_2) variable area flow meter/controllers (Cole-Parmer Inc.). The experiments were conducted in an indoor aquarium room; to minimize the potential for acidification of control aquaria due to atmospheric CO_2 build up in the room, the air was drawn from outside the aquarium room. To describe the carbonate system and the pCO_2 level, the pH was measured daily throughout the experiment using a Mettler-Toledo pH meter (NBS scale, calibrated with Mettler-Toledo buffers at pH4, pH7 and pH 10; every day prior to measurement of seawater pH). Every two days, total alkalinity was measured by potentiometric titration using the Gran Plot method [40], and checked against seawater reference materials (Batch 98, A.G. Dickson, Scripps Institution of Oceanography). The total alkalinity reading obtained from the reference materials (measured one time in every series of titrations) showed an accuracy that deviated 0.13% to 1.62% from the manufacturer's value. All carbonate chemistry parameters for each experimental tank were calculated from the measured values of temperature, pH, salinity and total alkalinity using the CO2SYS program [41] using the values for carbonic acid dissociation constants K_1* and K_2*of Millero [42].

The newly hatched trochophore larvae (~12 h post-fertilization) were divided into 20 groups and randomly assigned into treatment and control culture tanks. There were 20 tanks in total (4 treatments including control ×5 biological replicate tanks; each tank provides an independent sample of multiple tubeworms for analyses). Each tank received ~3500 larvae (2 larvae ml^{-1}). Larvae were reared in plastic tanks containing 1.7 L of 0.22 µm filtered seawater using optimal food concentration (1.8×10^5 cells $mL^{-1}$of *Isochrysis galbana*; in 10 folds greater than the optimum concentration of 1.8×10^4 cells mL^{-1} [43], this ensure unlimited development of the tubeworm larvae by food supply), temperature (25°C) and salinity (33–34 ppt) [34], culture water was renewed every other day. Once larvae reached competency to settle (attach) and metamorphose into juvenile tubeworms, i.e. 5 days, they were induced to attach on plastic surface using an artificial inducer of attachment, 10^{-4} M IBMX [33]. This well-known inducer was used instead of natural inducers such as biofilms in order to synchronize larval attachment and metamorphosis as well as to trigger the calcification immediately after metamorphosis especially at the lowest pH treatment levels where natural calcification is delayed [32]. Larvae that successfully attached and metamorphosed with calcareous tubes were kept in the respective treatment and culture conditions for 9 days, after which the calcareous tubes were collected for tube structure, composition and mechanical property analyses.

Preparation of samples for tube analyses

Fine powder, fractures and cross-sections of tube samples were prepared for structural analysis using X-ray powder diffraction (XRD), Fourier transform infrared spectrometry (FT-IR), scanning electron microscopy (SEM) and nanoindentation. Individuals were first rinsed with double-distilled water to remove salts, dislodged from the substrate and then preserved in 75% ethanol. Soft organic tissues were removed by immersing the tubeworms in 5% bleach (NaOCl, Clorox^{TM}) for about 20 minutes [44]. These tissue free tubes were processed further into fine and homogenous powder for XRD and FT-IR analyses. Grinding was performed in a 75% ethanol medium to minimize structural damage caused by over-grinding [45], glass microscope slides were used to provide a non-adhesive surface on which the slurry samples were air-dried overnight. Weighing papers sachets were used to store the powder samples (1–18 mg, at 20–24°C) until analysis.

Tube fractures and sections were prepared for ultrastructure analysis using scanning electron microscope (SEM). To create fractured surfaces, tissue free tube samples were frozen for 30 seconds in liquid nitrogen, and then immediately crushed using fine forceps to reduce grinding action during fracture. To prepare sections, tubes were embedded in resin, and then sectioned perpendicular to the long axis of the tube exposing the cross-sectional surfaces using a handmade low speed saw in the hard tissue laboratory of the Prince Philip Dental Hospital, Hong Kong. After locating the cross-sectional surface, excess surrounding resins were trimmed away to produce a small sectioned area suitable for ultramicrotomy [46]. Smooth, polished surfaces were obtained using an ultramicrotome to remove thin (85 nm thick) sections (Ultracut S, Leica), and the surface was etched in 1% acetic acid solution for 10 second to reveal topographical details of the microstructures prior to SEM.

Analysis of tube composition

Relative proportion of calcite, aragonite, and amorphous $CaCO_3$ (ACC) content in tube samples was qualitatively and semi-quantitatively analyzed using XRD and FT-IR. In the XRD samples, a known quantity of calcium fluoride (CaF_2) was mixed with powder tube samples as an internal standard [47]. XRD spectrum and data were obtained using a Bruker D8 Advance X-ray powder diffractometer equipped with a Cu Kα radiation and a LynxEye detector. The system was calibrated by Standard Reference Material 660a (lanthanum hexa boride, LaB_6), obtained from the U. S. National Institute of Standard and Technology, for the line position. The diffractometer was operated at 40 kV and 40 mA, and the 2θ scan range was from 10° to 110°, with a step size of 0.02° and a scan speed of 0.3 s/step. Qualitative phase identification was performed using Eva XRD Pattern Processing software (Bruker Co. Ltd.) by matching powder XRD patterns with those retrieved from the standard powder diffraction database of the International Centre for Diffraction Data (ICDD PDF-2 Release 2008). The Rietveld refinement method for quantitative analysis of the phase compositions was processed by the TOPAS (version 4.0) crystallographic program [48].The elemental proxy of calcite mineral in tube samples, the magnesium/calcium ratio, was also measured using the housed EDS system in SEM in order to corroborate the results of XRD.

ACC content was quantified using the intensity ratio of carbonate ion infrared absorption bands, $I_{max}v_2/I_{max}v_4$, using FT-IR [16,49]. To obtain infrared absorption spectra, powdered samples (~1 mg) were mixed with KBr (~10 mg; dehydrated at 98°C overnight). This mixture was pressed into a 13 mm diameter pellet (at 9 tons; for 2 min). Fourier transform infrared spectrometer (FT-IR, L120-000B, Perkin Elmer, USA) was used to obtain the spectrum ranging from 500–2000 cm^{-1} with 1 cm^{-1}resolution. The spectra were baseline corrected using Origin Pro Version 8.5. Second order derivatives were obtained by the Savitzky-Golay smoothing method before the peak heights at 855 cm^{-1} (v_2) and 713 cm^{-1} (v_4) corresponding to the internal vibration modes of CO_3^{2-} ions in aragonite were measured. The ratio of the maximal intensities of the v_2 versus the v_4 absorption bands $I_{max}v_2/I_{max}v_4$ was quantified to determine the effect of pH/pCO_2 on ACC content in tubes.

Tube ultrastructure was examined in fractured and cross-sectioned samples using SEM. Tube sections and fractures were mounted onto aluminum stubs with carbon tape and were sputter coated with gold – palladium alloy (~50 nm) prior to SEM study. Specimens with poorly conductive resin were surrounded with silver paint to avoid electron charging. SEM analysis was performed using Leo 1530 FEG SEM, equipped with an Inca EDX system [50]. To validate the observed difference in calcite content, Mg/Ca ratio, also the known elemental proxy of calcite was calculated from the ratio of elemental Mg and Ca composition obtained from EDX measurement (at 20 kV) from 15 random points on the fractured surfaces [51].

Tube mechanical strength

Tube mechanical properties, hardness and elasticity, were measured using nanoindentation. After SEM imaging, resin embedded specimens were further cut with a diamond knife to remove thin (85 nm thick) sections with an ultramicrotome (Ultracut S, Leica). This removed the gold-palladium alloy coating use in the SEM analysis, and also smoothed the surface topography for nanoindentation testing. Specimens were tested dry in ambient conditions using a triboindenter (Hysitron Inc., USA) equipped with in-situ scanning probe microscopy (SPM) imaging for topographic imaging of residual impressions. For each specimen, measurements were taken from at least six random locations of the tube section. Attention was paid to avoid measurements from the bottom adhering structures of the tube, which can have distinctive mineralogy and architectures as shown in other calcifiers like barnacles [52]. Dynamic load and displacement of the quartz Berkovich three-sided pyramid indenter was monitored at a load resolution of <1 nN and displacement resolution of 0.1 nm. Specimens with little surface roughness were indented with controlled peak loads between 500 to 7000 μN, in order to achieve necessary depth of penetration from 130 to 700 nm that minimizes the error in determining of contact area between the indenter and the specimen [53]. The applied load function was divided into three segments: the first segment was a loading phase with a standard loading time of five seconds, the second segment was a hold period of three seconds, and the third segment was an unloading phase with decreasing load at the same rate as first segment until zero force was reached. Hardness (H) and elastic modulus (E) generated from the recorded load-displacement curves were recorded after each measurement [54].

Data analysis

The effect of elevated pCO_2 on the tube composition and mechanical properties were assessed using one factor analysis of variance (ANOVA). Before the analysis, data were checked for ANOVA assumptions such as normality and heterogeneous expectations using Shapiro–Wilk's and Fligner-Killeen tests, respectively. If the ANOVA test showed a significant difference among treatments, the Dunnett test was used to compare the effect of each pCO_2 treatment compared with the control. Carbonate

system parameters were analyzed for differences among treatments using one-way ANOVAs and post-hoc Tukey HSD tests.

Results

CO_2 perturbation and carbonate chemistry

The measured and calculated carbonate system parameters during the study period are shown in Table 1. As expected, there was a significant difference in pH, pCO_2 and aragonite saturation (Ω_A) levels between the control and the given treatment conditions (ANOVA: pH, $F_{3,\ 16} = 61.445$, $p<0.001$; Ω_A, $F_{3,\ 16} = 96.971$, $p<0.001$). The Ω_A in the culture tanks of the pH 7.6 and 7.4 treatment groups were near and below saturation levels, respectively. However, there was no significant difference in salinity, total alkalinity and temperature among control and treatments (one-way ANOVA: Salinity; $F_{3,\ 16} = 1.071$, $p>0.05$; total alkalinity, $F_{3,\ 16} = 4.482$, $0.01<p<0.05$; temperature, $F_{3,\ 16} = 2.339$, $p>0.05$; Tukey post hoc test; $p>0.05$ for all comparisons of experimental groups). The daily pH measurements and subsequent calculation of the carbonate chemistry parameters indicated that the carbonate system within and among treatment tanks was relatively stable throughout the experiment (Figure 1). The number of algal cells used to feed larvae or juveniles did not significantly affect aragonite saturation level (Figure S1). Such a stable carbonate system via experimental CO_2 perturbation allowed us to examine the effects of high pCO_2 on tube composition, ultrastructure and mechanics.

Tube composition

The XRD diffraction peaks corresponding to the tube mineral indicated the presence of mixture phases of aragonite and structure of low-Mg calcite. The calcite main peak 2θ position at 29.4 degree is consistent with a calcite structure with low Mg occupancy. In ambient seawater chemistry conditions (control), the juvenile tube was predominantly composed of aragonite with negligible calcite content (Figure 2a), with a calcite/aragonite ratio of ~0.008. Surprisingly, this ratio increased by 2 to 3 times at elevated pCO_2 levels, i.e. pH 7.6 and 7.4 (Figure 2b; ANOVA results: $F_{3,\ 16} = 6.77$, $p<0.05$). However, the relative proportion of aragonite and calcite in the tube was not affected by the near future pCO_2 level of pH 7.9. This increase in calcite content at elevated pCO_2 conditions was also confirmed using the energy-dispersive X-ray spectroscopy (EDS or EDX) analysis of magnesium to calcium ratio. The Mg/Ca ratio in tube, an elemental indicator for calcite, also increased with decreasing pH or aragonite saturation level (Figure 3; Spearman Rank Correlation Test result: $R_{spearman} = -0.58$, $p<0.05$).

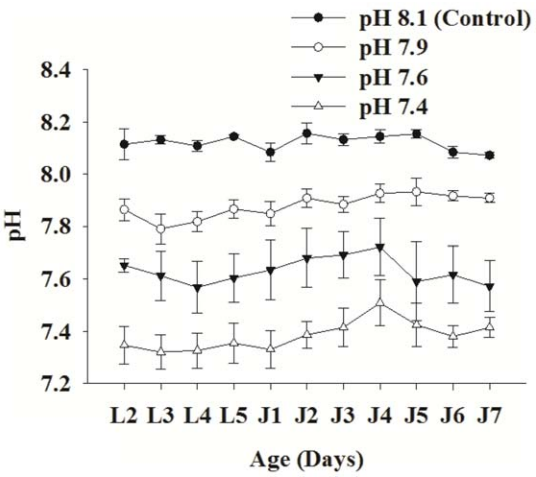

Figure 1. Variation of pH (NBS scale), a proxy of carbonate system, in control and among pH/pCO_2 treatment culture tanks during the experiment. Each data point represents mean ± SD of 5 biologically independent measurements, pH levels are statistically different with p-value<0.05. Abbreviations: L1–L5, Day 1–5 of larval phase; J1–J7, Day 1–7 of juvenile phase.
doi:10.1371/journal.pone.0042718.g001

The FT-IR spectra of the tube built by the tubeworm at ambient seawater condition is shown in Figure 4a.The IR peaks at 855 cm^{-1} and 713 cm^{-1} were assigned as ν_2 and ν_4 absorption bands of the carbonate groups of the crystalline $CaCO_3$, respectively [16]. The intensity ratio of ν_2 to ν_4 was used to quantify the amorphous $CaCO_3$ content (ACC) in the tube (Figure 4b). The ratio ranged between 2.5 to 3 for the tubes obtained from the ambient condition. The high pCO_2 treatments

Table 1. Measured and calculated values (mean ± SD, n = 5) of environmental and carbonate system parameters for the ambient (control) and the three pH/pCO_2 treatments before sample collection for shell structure, composition and mechanical strength measurement at two monitoring time points, day 5 juvenile/J5 and day 7 juvenile/J7.

	Measured parameters				Calculated parameters	
CO_2 Treatment	pH	Salinity ppt	Temp °C	TA (μmol/kg-SW)	pCO_2 (μatm)	Ω_A
Day 5						
Control	8.05±0.03	34.8±1.2	25.6±0.1	2160±71	539±42	2.5±0.3
Low	7.88±0.04	34.5±1.1	25.6±0.1	2293±97	874±88	1.8±0.2
Medium	7.67±0.04	35.3±0.8	25.6±0.1	2262±48	1530±142	1.2±0.1
High	7.34±0.08	34.5±1.1	25.6±0.1	2326±70	3548±675	0.6±0.1
Day 7						
Control	8.08±0.02	34.4±0.5	25.6±0.2	2210±112	514±27	2.7±0.2
Low	7.89±0.03	34.5±0.6	25.1±0.5	2212±60	852±75	1.8±0.1
Medium	7.58±0.11	34.2±0.8	25.4±0.3	2346±106	2041±592	1.1±0.2
High	7.37±0.14	33.7±1.0	25.6±0.3	2356±41	3438±982	0.7±0.2

TA, total alkalinity of seawater; pCO2, partial pressure of CO2; ΩA, aragonite saturation state.
doi:10.1371/journal.pone.0042718.t001

significantly increased the ACC content in the tube (Figure 4c; ANOVA results: $F_{3,\ 14} = 20.01$, $p<0.001$). Although the tube ACC content at the pH 7.9 was statistically similar to the ambient pH 8.1, the two low pH treatments 7.6 and 7.4 had significantly higher amount of ACC (Figure 4c).

Tube ultrastructure

The scanning electron micrograph (SEM) of tubeworm tube ultrastructure is shown in Figures 5 and 6. Using the recently established terminology and description for the tubeworm tube ultrastructure analysis [55], three distinguishable layers were observed in the juvenile tubeworm tube raised at ambient pH 8.1. The tube is coated by the outermost layer of spherulitic prismatic structure (SPHP), the middle layer composed of rounded homogeneous crystal structure (RHC), and the innermost layer is made of an irregularly oriented prismatic structure (IOP).Unlike adult tubes, the juvenile tubes examined in this study did not have a prominent SPHP layer (Figure 5a). Tube sections as well as fractures had all the three layers (Figures 5a and 6a). The high pCO_2 had a significant impact on the tube ultrastructure. For example, tubes produced at the pH treatments 7.6 and 7.4 had higher porosity and layer irregularity with more signs of pitting (Figures 5c and d; Figures 6c and d). At all the three high pCO_2 treatments, the IOP layer contained less structured crystallites and thus this layer became indistinguishable from the rounded crystallites observed in RHC layers (Figures 5c and 6d). Under low pH conditions, the crystallites within RHC layer appeared as amorphous cryptocrystalline masses (Figure 5d and 6d).

Tube mechanical properties

The tube portions where hardness and elasticity measurements were made at different position along the cross sectional surface of the tube as shown in Figure 7a and the typical mark created by the indentation is shown in Figure 7b. At ambient conditions, the tube hardness (H) was 2.36±0.27 GPa and the stiffness (E) was 39.94±3.85 GPa. These two mechanical properties of a tube were significantly affected by high pCO_2. At pH 7.4, the hardness and the stiffness were reduced by as much as 72% ($F_{3,8} = 4.688$, $p<0.05$) and 62% ($F_{3,8} = 4.421$, $p<0.05$), respectively (Figures 8a and b).

Discussion

In highly productive coastal and estuarine waters, an anthropogenically imposed or naturally decreasing carbonate ion supply due to ocean acidification and/or eutrophication (including hypoxia and upwelling) may hinder or disrupt the calcification of a variety of marine organisms possibly by making this key physiological process more expensive [24,56–58]. Early life stages such as larvae and newly metamorphosed juvenile stages are particularly vulnerable to this unprecedented OA stress due to their high dependence on their environment to provide the appropriate conditions [59–65]. Few recent studies on calcifying animals have made pioneering observations on crystallography of calcified structures produced at high pCO_2, including measurements of the elemental calcite/aragonite ratio and microhardness of skeletons [19,20,22,66]. According to these studies, OA has damaging impacts not only to calcification rate but also to the microstructures and crystallographic textures of calcareous products. Organisms are thus faced with twin OA threats, i.e. decreased calcification and abnormal tube microstructure. It is therefore likely that the intensively calcifying juvenile tubeworms will not have the ability to produce a calcareous protective tube with normal structural integrity and mechanical properties when exposed to OA conditions projected for the year 2100 and beyond. This study tested this hypothesis by simultaneously measuring mineral composition, ultrastructures and mechanical properties of $CaCO_3$ tubes produced by tubeworms at various OA scenarios finding that high pCO_2 treatments altered tube composition, structure, and hardness. This study also provides a comprehensive analysis of tube mineralogy produced by early juveniles of the important biofouling tubeworm, *Hydroides elegans*.

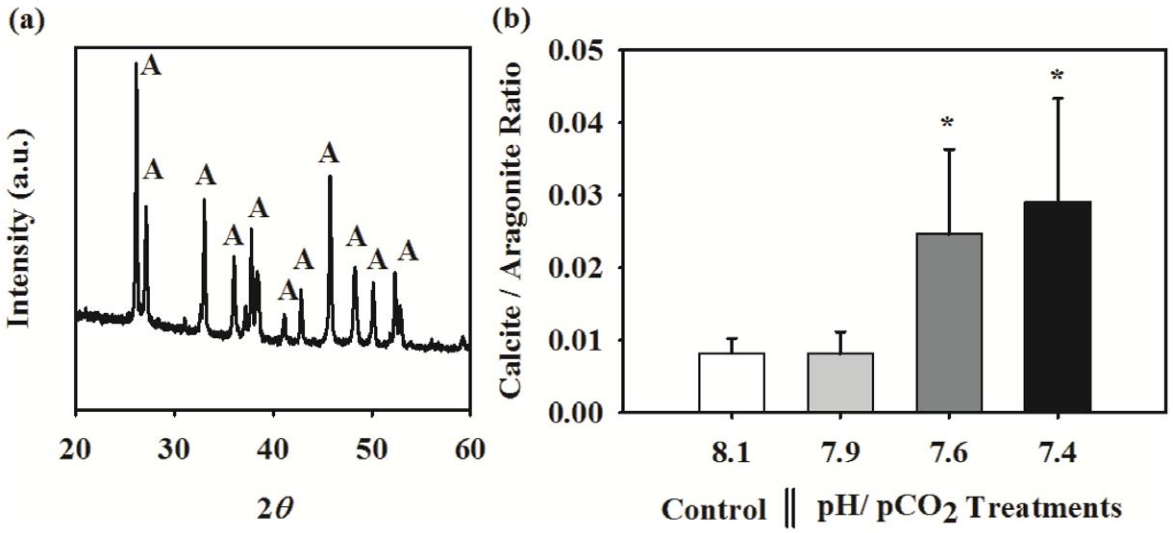

Figure 2. Effects of pH/pCO_2 on shell mineralogy in the juvenile tubeworm, *Hydroides elegans*. (a) The X-ray diffraction pattern of shell obtained from the control pH/pCO_2 (pH 8.1) showing the presence a set of diffraction peaks resulting from the presence of the dominating aragonite (A) phase. (b) Effect of pH/pCO_2 on the shell calcite/aragonite ratio, which was quantified from the X-ray diffraction analysis. Each bar represents the mean ± SD of 5 biologically independent measurements each obtained from independent culture. The asterisk (*) shown on the bar indicates a significant difference between the control and the treatment according to the Dunnett's Post-hoc test ($p<0.05$).
doi:10.1371/journal.pone.0042718.g002

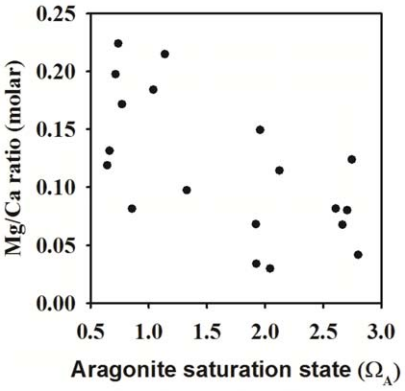

Figure 3. The relationship between aragonite saturation state and the tube magnesium to calcium (Mg/Ca) ratio. The strength of the relationship was analyzed using the Spearman's rank-order correlation coefficient.
doi:10.1371/journal.pone.0042718.g003

Tube mineralogy: Influence of OA

At ambient pH, the tube is primarily made of the more soluble $CaCO_3$ polymorph, aragonite, appearing as needle-like prismatic crystallites; and had only a trace amount of the most stable crystalline form of $CaCO_3$, calcite. There was also a small but detectable amount of an unstable amorphous form of $CaCO_3$, ACC. In contrast, tubes produced by adult tubeworms, *H. dianthus*, *H. norvegicus* or *H. spongicola* had both aragonite and calcite in comparable quantities and thus produced bimineralic calcareous tubes [20,67,68]. In tubeworms, there appeared to be an ontogenetic shift from preferentially calcifying aragonite from ACC in the early juvenile, and then both calcite and aragonite from the ACC precursor in adults (Vinn, personal communication). However, this hypothesis is yet to be confirmed in serpulid worms, although the production of calcite or aragonite from the ACC precursor is very common in marine organisms such as molluscs and echinoderms [12,15].

The most unexpected finding was that the composition of the aragonite dominated bimineralic calcareous tube produced by the juvenile tubeworm is strongly dependent on Ω_A. In the highest two pCO_2 treatments, when Ω_A was near or below one, the tube had significantly higher proportion of calcite (Figure 2b). The EDX-SEM analysis of Mg/Ca ratio (Figure 3) reconfirmed that calcite content increased in response to decreasing Ω_A. The aragonite to calcite ratio appears to be a phenotypically plastic trait in tubeworms changing with the seawater chemistry. In corroboration with our results, a whelk and another species of a tubeworm had higher calcite/aragonite ratio in Ω_A under-saturated conditions [20,69]. These results can be interpreted as a consequence of preferential dissolution of the more soluble aragonite [20]. Aragonite generally tends to dissolve at a much faster rate near or below Ω_A [30]. Juvenile worms of the *H. elegans* are under particularly high risk at low Ω_A because (1) calcareous tubes are produced from glands located under the unfolded collars, a calcification site that is semi-exposed to the external environment [70] and (2) the outer surface of the tube structure is protected only by a relatively thin organic layer when compared to bivalves, urchins and corals [20].

In addition to the direct dissolution threat, aragonite production also has a greater energetic requirement than calcite [71]. Accreting aragonite is more costly because it has higher packing density of 2.95 gcm^{-3}, while that of calcite is only 2.72 gcm^{-3} [26]. Additionally, aragonite is constructed with expensive organic

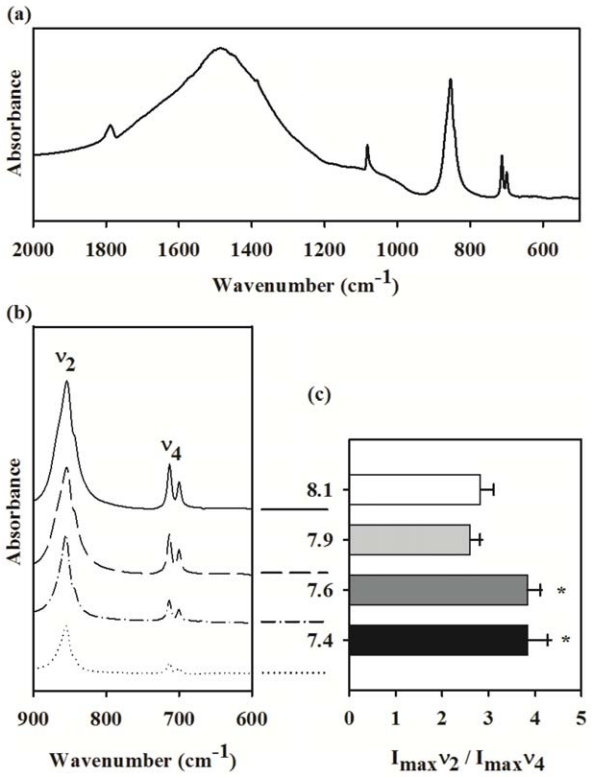

Figure 4. Effects of pH/pCO_2 on shell mineralogy in the juvenile tubeworm, *Hydroides elegans*. (a) The infrared absorption spectrum obtained from shell samples of the control pH/pCO_2 (pH 8.1) using the Fourier transform infrared spectrometry (FT-IR). (b) Effects of pH/pCO_2 on the magnified portion, between wavelengths 600–900 cm^{-1}, of infrared spectral pattern of the shell. (c) Effect of pH/pCO_2 on the intensity ratio (I_{max}) of the two absorption peaks at 855 cm^{-1} (ν_2) and 713 cm^{-1} (ν_4). The $I_{max}\nu_2/I_{max}\nu_4$ ratio is an indicator of amorphous calcium carbonate (ACC) content. Each bar represents the mean ± SD of 5 biologically independent measurements. The asterisk (*) shown on the bar indicates a significant difference between the control and the treatment according to the Dunnett's Post-hoc test ($p<0.05$).
doi:10.1371/journal.pone.0042718.g004

matrix proteins often in larger quantity than calcite [72]. Since the basic metabolic demands for cellular maintenance, such as ion regulation and protein synthesis, may be increased at low pH [66,73], budgeting enough energy for aragonite accretion may not be possible. Although the degree of plasticity in polymorph production of these bimineralic calcifiers is still uncertain, calcifying more calcite may be a preferable strategy to enable more economical calcification and better resistance to dissolution in low pH environments. However, the preferential use of calcite as a defense against dissolution should be, at this stage, advanced with caution; because the solubility of this biomineral is also greatly dependent on the crystal sizes and the quantity and nature of organic matrices.

The FT-IR analysis showed an interesting phenomenon, in that the ACC content in the tube increased by 20 to 30% at near or below aragonite saturation. While no certain explanation for this relationship between ACC content and decreasing Ω_A can be established by this work, ACC is a known precursor to both aragonite and calcite [49] and increased ACC content at low pH could reflect an increased calcification effort in this tubeworm. Increasing the ACC content may be an attempt to elevate production of crystalline products, i.e. calcite and/or aragonite. Our result showed a change in composition of tubes at pH 7.4,

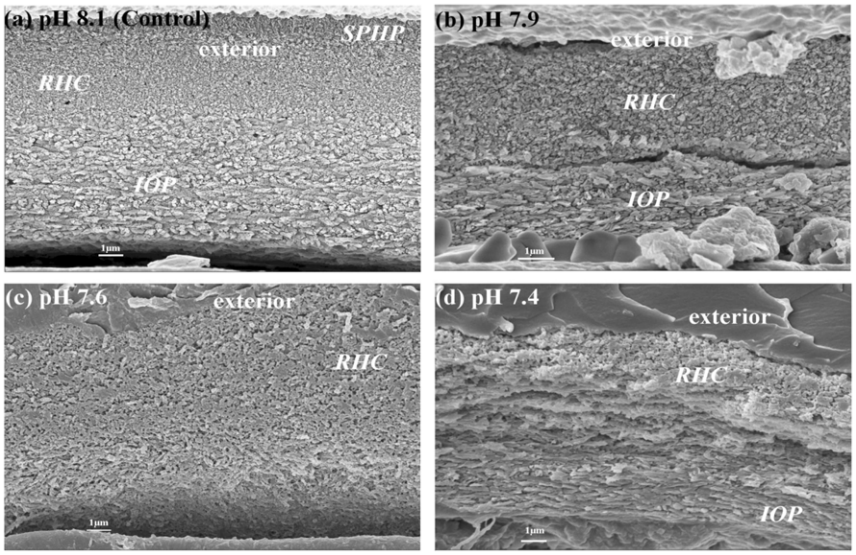

Figure 5. Effects of pH/pCO_2 on cross sectional views of the tube ultrastructures in the juvenile tubeworm, *Hydroides elegans*. Abbreviations: SPHP, spherulitic prismatic structure; IOP, irregularly oriented prismatic structure; RHC round homogenous crystal structure.
doi:10.1371/journal.pone.0042718.g005

while the animals at pH 7.9 and 7.6 were comparable to the ambient control conditions of pH 8.1. This similarity in treatment effects, however, should be comprehended with caution because of low replication numbers limiting statistical power.

Greater energetic costs in stressful environments, often interpreted as compensatory efforts against corrosive OA environments, are observed as changes in respiration and metabolic activity (in copepods) [74]. It has also been shown that nacre surface can be maintained in corrosive calcification fluid when food levels were increased [75]. The observed changes in skeleton composition such as Mg/Ca ratio can also be a result of altered physiology, which alters the materials for building up mineral products. When Mg/Ca levels were measured in similar OA studies, a reduction of Mg/Ca was found in a coral and echinoderms [76,77], while Mg/Ca was independent from pCO_2 levels in foraminifera, both findings contrast with the increase in Mg/Ca ratio observed in *H. elegans*. These discrepancies can be a result of variations in calcification pathways, since the fractionation of Mg/Ca in skeletons is determined by the mechanism of biomineralization [78]. The tubeworm in this study produces both calcite and aragonite, so the dissolution of aragonite which causes more calcite component to remain in the skeletal structure, can lead to a higher Mg/Ca as calcite generally incorporates more Mg in the lattice structure [79].

Mg/Ca ratio is recognized to correlate with certain environmental conditions, specifically with water temperature [80,81], and sometimes salinity [82]. Both temperature and salinity have been maintained constant in the course of this study, so it is

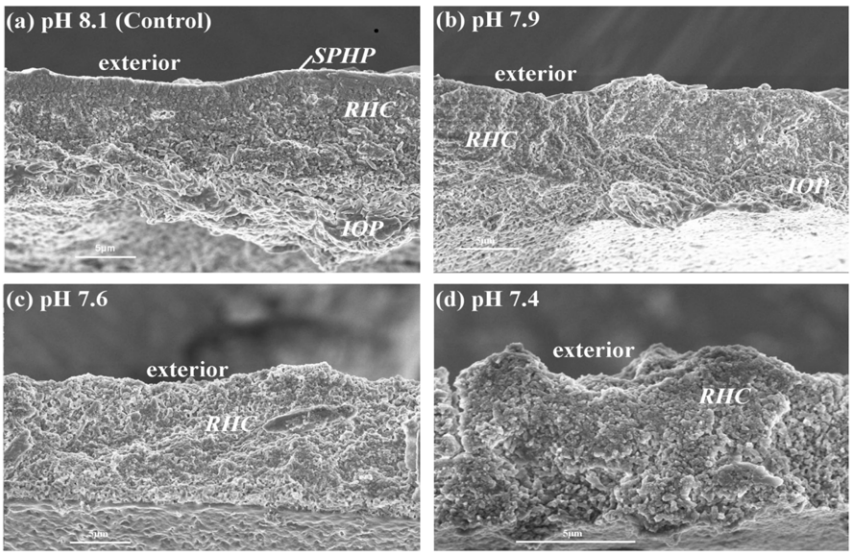

Figure 6. Effects of pCO_2 on fracture surfaces of the tube ultrastructures in the juvenile tubeworms, *Hydroides elegans*. Abbreviations: SPHP, spherulitic prismatic structure; IOP, irregularly oriented prismatic structure; RHC round homogenous crystal structure.
doi:10.1371/journal.pone.0042718.g006

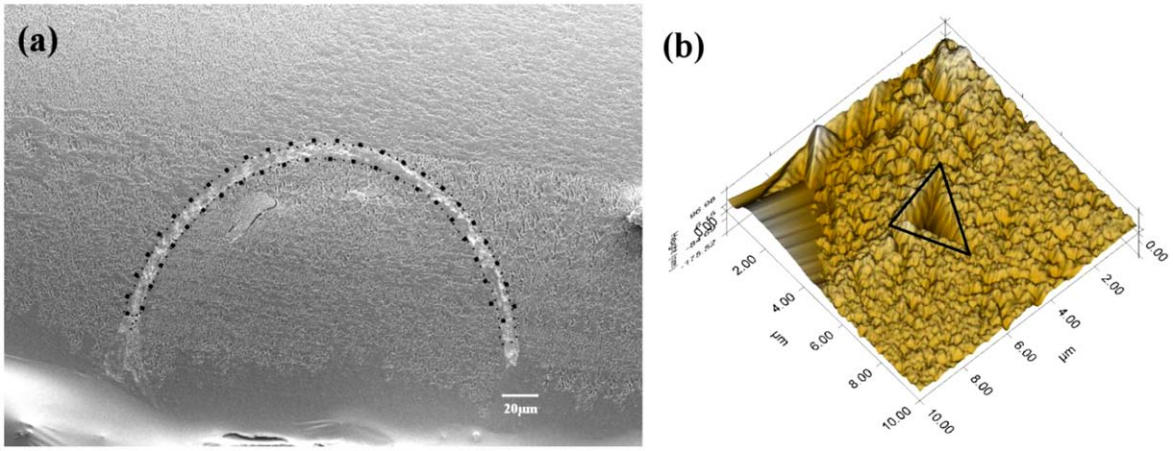

Figure 7. The tube portion used for nanoindentation analysis. (a) Portions of cross-sectional surfaces subjected to of nanoindentation test, at least six random points were tested over the tube area (surrounded by dotted line). (b) A mark created after indentation test from a shell sample of the control pH/pCO_2 (pH 8.1).
doi:10.1371/journal.pone.0042718.g007

reasonable to expect that environmental pH may influence the Mg/Ca ratio in the shell. Cellular acid-base balance and energy metabolism are known to be sensitive to pH alteration in the environment [83], these altered physiological processes may in turn affect shell morphology and composition including Mg/Ca ratio, for example known in foraminifera [84]. This interaction between seawater carbonate chemistry and the ultimate shell features, and how they interact with, or are affected by, the animal's physiology and intracellular environment should be explored further in marine organisms.

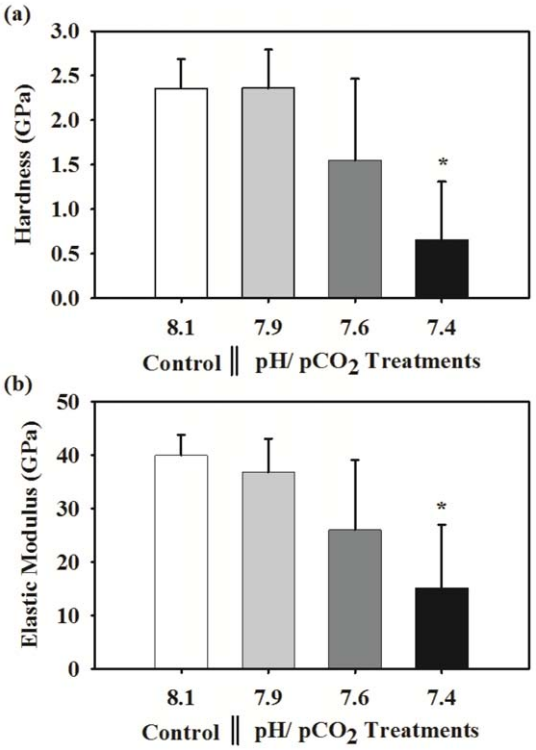

Figure 8. Effects of pH/pCO_2 on the shell hardness and elastic modulus in the juvenile tubeworm, *Hydroides elegans*. Each bar represents the mean ± SD of 4 to 2 biologically independent measurements; i.e. n = 4 for control, n = 3 for the pH 7.9 and 7.6, and n = 2 for the pH 7.4. This uneven biological replicates across treatments was due to loss of samples during hardness measurement. However, the Dunnett test is robust and suitable for the comparison of the mean obtained from uneven sample size. The asterisk (*) shown on the bar indicates a significant difference between the control and the treatment according to the Dunnett's Post-hoc test ($p<0.05$).
doi:10.1371/journal.pone.0042718.g008

Tube ultrastructure: Influence of OA

The calcareous tube produced by the juvenile tubeworm consists of three distinct textural layers: the outer, middle and inner layers namely spherulitic prismatic structure (SPHP), rounded homogeneous crystal structure (RHC) and irregularly oriented prismatic structure (IOP) respectively. The unoriented RHC and IOP layers usually have low density and weak mechanical resistance. In contrast, the outer most, oriented, SPHP layer is made of densely and orderly packed crystallites effectively protecting the underlying fragile tube structures from dissolution and external attacks [85]. A tube built without thick SPHP is also prone to the propagation of cracks [67].

The OA treatments dramatically affected the orientation, orderly structure and thickness of each of these three mineralized layers (Figures 5 and 6). Although the precise quantitative relationship between OA and tube ultrastructure (e.g. layer thickness and porosity) was not determined in this study, tubes made at all the three low pH treatments showed clear signs of dissolution of the protective SPHP layer, and also appeared to have increased pitting and a more open packing. Both the inner unoriented layers, RHC and IOP, showed a noticeably degraded crystalline structure under OA conditions. The RHC layer appeared corroded with pitting and less densely packed crystals at the lowest pH (Figures 5d & 6d). A similar change in crystallite morphology in response to reduced Ω_A in the calcification fluid, influenced by the external Ω_A, was observed in oysters [20,86], corals [19], bivalves [87] and the pearl oyster [31]. Under lower internal Ω_A, nucleation and growth of $CaCO_3$ crystallites was negatively affected in corals and resulted in shorter, wider and more faceted crystallites [19]. It may be the case in our observations that the semi-exposed nature of the calcification site resulted in reduced aragonite saturation, resulting in pitting and poorly ordered crystallites as in the aforementioned studies.

Tube mechanical properties: Influence of OA

Tube hardness and elasticity of the biofouling tubeworm, *Hydroides elegans*, in response to OA was impaired, with reductions in hardness and elasticity of 72% and 62%, respectively. These changes likely result from the disorganized ultrastructure and higher proportion of calcite (or less aragonite) in tubes produced in Ω_A undersaturated condition (pH 7.4) [26]. Similar reductions in mechanical properties were found in juvenile oysters [22,66], the California mussel, *Mytilus californianus* [88], and the pearl oyster [31]. Similar dissolution of aragonite has also been found in Antarctic bivalves [87], such a change in aragonite crystallography and mineralogy also strongly affects the material's hardness and mechanical properties [89].

The observed reduction in tube hardness and elastic modulus can be attributed to either 1) reduced aragonite content of the tube (i.e. reduced calcite/aragonite ratio) or 2) concurrent increase in elemental Mg/Ca ratio) or 3) impaired or altered tube ultrastructure (or increased tube porosity). Aragonite rich calcareous structures are found to have a higher hardness and elasticity than that of calcite dominated crystal structures [90,91]. In addition, layered structures are generally harder [92–94]. Therefore it is reasonable to speculate that *H. elegans* tubes will produce weaker and less elastic tubes under projected OA conditions due to decreased aragonite content and inability to produce multi-layered calcareous structures. According to recent studies, hardness of calcareous structures also depends on organic matrix proteins occluded in the structure [95]. Therefore, OA may have also reduced hardness through various mechanisms, yet results of the present study are insufficient to isolate the cause of such reduction in shell strength.

Although the organic matrix has been reported to show little response to OA in bivalves [31,96], this ability may be species specific. Both the quality and quantity of organic contents play a crucial role in governing shell formation, and the overall mechanical properties [97]. Thus near or below saturation levels of seawater could pose an important mechanical challenge to tubeworm juveniles. As a consequence of this poorly assembled and fragile tube, juvenile tubeworms may not be able to withstand physical disturbances and predation in the future ocean. In the face of these unprecedented threats, future studies should investigate this biomineral-environment interaction in long-term CO_2 perturbation experiments involving juveniles as well as adults with special attention to the potential ecological consequences of the altered mechanical properties. Ultimately, a tubeworm's ability to maintain a tube with the appropriate compositions of the particular polymorphs and elemental ratio for the necessary mechanical properties may be affected by low pH, and might subsequently determine their performance as pCO_2 increases.

Supporting Information

Figure S1 Effects of algae concentration on aragonite saturation state after 24 h and 48 h. This additional experiment without larvae examined the influence of three algal concentrations (0 cell/mL, 10^4 cells/mL, 10^5 cells/mL) on the aragonite saturation at four levels of pH (8.1, 7.9, 7.6, 7.4). Each bar represents the mean ± SD of 3 replicates. Three-way ANOVA: Algae; $F_{2,\ 48} = 1.607$; $p>0.05$; Algae*CO_2; $F_{6,48} = 1.444$; $p<0.05$; Algae*Day; $F_{3,48} = 0.183$; $p>0.05$; Algae*CO_2*Day; $F_{6,48} = 0.640$.
(TIF)

Acknowledgments

The authors would like to thank YY Chui for sectioning, HKU-EMU for SEM analysis and, VYL Fung for FT-IR measurement, KF Chan, Y He and CC Wong for nanoindentation measurement. We thank PY Qian, Mary Sewell, Gray Williams, David Dudgeon and Kenneth Leung for their valuable discussions during the course of this project. We also wish to thank Richard Zeebe, Ryuji Asami, Olev Vinn, Andrew Mount, Paul Taylor and Maggie Cusack for their highly valuable contribution during our biomineral analysis.

Author Contributions

Conceived and designed the experiments: VBSC VT. Performed the experiments: VBSC. Analyzed the data: CL YCW XWL ACL. Contributed reagents/materials/analysis tools: KS TZ. Wrote the paper: VBSC VT.

References

1. Zeebe RE, Zachos JC, Caldeira K, Tyrrell T (2008) Oceans: Carbon emissions and acidification. Science 321: 51–52.
2. Feely RA, Orr J, Fabry VJ, Kleypas JA, Sabine CL, et al. (2009) Present and future changes in seawater chemistry due to ocean acidification. Geophysical monograph 183: 175–188.
3. Fabry VOJ, McClintock JB, Mathis JT, Grebmeier JM (2009) Ocean acidification at high latitudes: the bellwether. Oceanography 22: 160–171.
4. Howarth R, Chan F, Conley DJ, Garnier J, Doney SC, et al. (2011) Coupled biogeochemical cycles: eutrophication and hypoxia in temperate estuaries and coastal marine ecosystems. Front Ecol Environ 9: 18–26.
5. Borges A, Gypens N (2010) Carbonate chemistry in the coastal zone responds more strongly to eutrophication than to ocean acidification. Limnol Oceanogr 55: 346–353.
6. Cai WJ, Hu X, Huang WJ, Murrell MC, Lehrter JC, et al. (2011) Acidification of subsurface coastal waters enhanced by eutrophication. Nature Geosci 4: 766–770.
7. Waldbusser G, Voigt E, Bergschneider H, Green M, Newell R (2011) Biocalcification in the eastern oyster (*Crassostrea virginica*) in relation to long-term trends in Chesapeake Bay pH. Estuaries and Coasts 34: 221–231.
8. Hadfield MG, Carpizo-Ituarte EJ, del Carmen K, Nedved BT (2001) Metamorphic competence, a major adaptive convergence in marine invertebrate larvae. Am Zool 41: 1123–1131.
9. Medaković D, Popović S, Gržeta B, Plazonić M, Hrs-Brenko M (1997) X-ray diffraction study of calcification processes in embryos and larvae of the brooding oyster *Ostrea edulis*. Mar Biol 129: 615–623.
10. Stenzel H (1964) Oysters: composition of the larval shell. Science 145: 155.
11. Addadi L, Raz S, Weiner S (2003) Taking advantage of disorder: amorphous calcium carbonate and its roles in biomineralization. Adv Mater 15: 959–970.
12. Politi Y, Metzler RA, Abrecht M, Gilbert B, Wilt FH, et al. (2008) Transformation mechanism of amorphous calcium carbonate into calcite in the sea urchin larval spicule. Proc Natl Acad Sci U S A 105: 17362–17366.
13. Auzoux-Bordenave S, Badou A, Gaume B, Berland S, Helléouet MN, et al. (2010) Ultrastructure, chemistry and mineralogy of the growing shell of the European abalone *Haliotis tuberculata*. J Struct Biol 171: 277–290.
14. Mount AS, Wheeler AP, Paradkar RP, Snider D (2004) Hemocyte-mediated shell mineralization in the eastern oyster. Science 304: 297–300.
15. Weiss IM, Tuross N, Addadi L, Weiner S (2002) Mollusc larval shell formation: amorphous calcium carbonate is a precursor phase for aragonite. J Exp Zool Part A 293: 478–491.
16. Beniash E, Aizenberg J, Addadi L, Weiner S (1997) Amorphous calcium carbonate transforms into calcite during sea urchin larval spicule growth. Proc R Soc Lond B Biol Sci 264: 461.
17. Mucci A (1983) The solubility of calcite and aragonite in seawater at various salinities, temperatures, and one atmosphere total pressure. Am J Sci 283: 780.
18. Comeau S, Jeffree R, Teyssié JL, Gattuso JP (2010) Response of the arctic pteropod *Limacina helicina* to projected future environmental conditions. PLoS ONE 5: e11362.
19. Cohen AL, McCorkle DC, De Putron S, Gaetani GA, Rose KA (2009) Morphological and compositional changes in the skeletons of new coral recruits reared in acidified seawater: Insights into the biomineralization response to ocean acidification. Geochem Geophys Geosyst 19: Q07005.
20. Ries JB (2011) Skeletal mineralogy in a high-CO_2 world. J Exp Mar Biol Ecol 403: 54–64.
21. Checkley Jr DM, Dickson AG, Takahashi M, Radich JA, Eisenkolb N, et al. (2009) Elevated CO_2 enhances otolith growth in young fish. Science 324: 1683.
22. Dickinson GH, Ivanina AV, Matoo OB, Pörtner HO, Lannig G, et al. (2012) Interactive effects of salinity and elevated CO_2 levels on juvenile eastern oysters, *Crassostrea virginica*. J Exp Biol 215: 29–43.
23. Marshall DJ, Santos JH, Leung KMY, Chak WH (2008) Correlations between gastropod shell dissolution and water chemical properties in a tropical estuary. Mar Environ Res 66: 422–429.

24. Pörtner HO (2008) Ecosystem effects of ocean acidification in times of ocean warming: a physiologist's view. Effects of ocean acidification on marine ecosystems. Mar Ecol Prog Ser 373: 203–217.
25. Findlay HS, Wood HL, Kendall MA, Spicer JI, Twitchett RJ, et al. (2009) Calcification, a physiological process to be considered in the context of the whole organism. Biogeosci Disc 6: 2267–2284.
26. Weiner S, Addadi L (1997) Design strategies in mineralized biological materials. J Mater Chem 7: 689–702.
27. Sikes CS, Wheeler AP (1986) The organic matrix from oyster shell as a regulator of calcification in vivo. Biol Bull 170: 494–505.
28. Bentov S (2010) Stabilization of amorphous calcium carbonate by phosphate rich organic matrix proteins and by single phosphoamino acids. J Struct Biol 171:207–215
29. Rodolfo-Metalpa R, Houlbreque F, Tambutte E, Boisson F, Baggini C, et al. (2011) Coral and mollusc resistance to ocean acidification adversely affected by warming. Nature Clim Change 1: 308–312.
30. Nienhuis S, Palmer AR, Harley CDG (2010) Elevated CO_2 affects shell dissolution rate but not calcification rate in a marine snail. Proc R Soc B 277: 2553–2558.
31. Welladsen HM, Southgate PC, Heimann K (2010) The effects of exposure to near-future levels of ocean acidification on shell characteristics of *Pinctada fucata* (Bivalvia: Pteriidae). Molluscan Res 30: 125–130.
32. Lane A, Mukherjee J, Chan V, Thiyagarajan V High-CO_2 threats to metamorphosing larvae of the tubeworm *Hydroides elegans*. Mar Biol. In press.
33. Nedved BT, Hadfield MG (2009) *Hydroides elegans* (Annelida: Polychaeta): A model for biofouling research. In: Flemming H-C, Murthy PS, Venkatesan R, Cooksey K, editors. Marine and Industrial Biofouling: Springer Berlin Heidelberg. pp. 203–217.
34. Qiu JW, Qian PY (1997) Combined effects of salinity, temperature and food on early development of the polychaete *Hydroides elegans*. Mar Ecol Prog Ser 152: 79–88.
35. Pechenik JA, Pearse JS, Qian PY (2007) Effects of salinity on spawning and early development of the tube-building polychaete *Hydroides elegans* in Hong Kong: not just the sperm's fault? Biol Bull 212: 151–160.
36. Riebesell U, Fabry VJ, Hansson L, Gattuso JP, editors (2010) Guide to best practices for ocean acidification research and data reporting: Luxembourg: Publications Office of the European Union.
37. Caldeira K, Wickett ME (2005) Ocean model predictions of chemistry changes from carbon dioxide emissions to the atmosphere and ocean. J Geophys Res 110: C09S04.
38. Dai M, Zhai W, Cai W-J, Callahan J, Huang B, et al. (2008) Effects of an estuarine plume-associated bloom on the carbonate system in the lower reaches of the Pearl River estuary and the coastal zone of the northern South China Sea. Cont Shelf Res 28: 1416–1423.
39. Hofmann GE, Smith JE, Johnson KS, Send U, Levin LA, et al. (2011) High-Frequency Dynamics of Ocean pH: A Multi-Ecosystem Comparison. PLoS ONE 6(12): e28983
40. Bradshaw A, Brewer P (1988) High precision measurements of alkalinity and total carbon dioxide in seawater by potentiometric titration - 1. Presence of unknown protolyte (s)? Mar Chem 23: 69–86.
41. Pierrot D, Lewis E, Wallace D (2006) MS Excel program developed for CO_2 system calculations. ORNL/CDIAC-105 Carbon Dioxide Information Analysis Center, Oak Ridge National Laboratory, US Department of Energy, Oak Ridge, Tennessee.
42. Millero FJ, Graham TB, Huang F, Bustos-Serrano H, Pierrot D (2006) Dissociation constants of carbonic acid in seawater as a function of salinity and temperature. Mar Chem 100: 80–94.
43. Qiu J, Qian P (1997) Combined effects of salinity, temperature and food concentration on the early development of the polychaete *Hydroides elegans* (Haswell, 1883). Mar Ecol Prog Ser 152: 79–88.
44. Taylor PD, Vinn O, Kudryavtsev A, Schopf JW (2010) Raman spectroscopic study of the mineral composition of cirratulid tubes (Annelida, Polychaeta). J Struct Biol 171: 402–405.
45. Bish DL, Reynolds R (1989) Sample preparation for X-ray diffraction. Reviews in Mineralogy 73: 20.
46. Dykstra MJ (1993) A manual of applied techniques for biological electron microscopy: Plenum Press. New York. US.
47. Snyder R, Bish DL (1989) Quantitative analysis. Reviews in Mineralogy 101: 20.
48. Larson A, Von Dreele R (2001) Los Alamos National Laboratory Report LAUR, 1994. J Appl Crystallogr 34: 210–213.
49. Raz S, Hamilton PC, Wilt FH, Weiner S, Addadi L (2003) The transient phase of amorphous calcium carbonate in sea urchin larval spicules: the involvement of proteins and magnesium Ions in its formation and stabilization. Adv Funct Mater 13: 480–486.
50. Jacob DE, Soldati AL, Wirth R, Huth J, Wehrmeister U, et al. (2008) Nanostructure, composition and mechanisms of bivalve shell growth. Geochim Cosmochim Acta 72: 5401–5415.
51. Dodd JR (1967) Magnesium and strontium in calcareous skeletons: a review. J Paleontol 41: 1313–1329.
52. MacDonald J, Freer A, Cusack M (2010) Attachment of oysters to natural substrata by biologically induced marine carbonate cement. Mar Biol 157: 2087–2095.
53. Sumitomo T, Kakisawa H, Kagawa Y (2011) Nanoscale structure and mechanical behavior of growth lines in shell of abalone *Haliotis gigantea*. J Struct Biol 174: 31–36.
54. Merkel C, Deuschle J, Griesshaber E, Enders S, Steinhauser E, et al. (2009) Mechanical properties of modern calcite- (*Mergerlia truncata*) and phosphate-shelled brachiopods (*Discradisca stella* and *Lingula anatina*) determined by nanoindentation. J Struct Biol 168: 396–408.
55. Vinn O, Tenhove HA, Mutvei H (2008) On the tube ultrastructure and origin of calcification in sabellids (Annelida, Polychaeta). Palaeontology 51: 295–301.
56. Wood HL, Spicer JI, Widdicombe S (2008) Ocean acidification may increase calcification rates, but at a cost. Proc R Soc Lond B Biol Sci 275: 1767.
57. Hofmann GE, Todgham AE (2010) Living in the now: physiological mechanisms to tolerate a rapidly changing environment. Annu Rev Physiol 72: 127–145.
58. Doney SC, Fabry VJ, Feely RA, Kleypas JA (2009) Ocean acidification: the other CO_2 problem. Ann Rev Mar Sci 1: 169–192.
59. Albright R (2011) Reviewing the effects of ocean acidification on sexual reproduction and early life history stages of reef-building corals. Population 12: 15.
60. Kurihara H (2008) Effects of CO_2-driven ocean acidification on the early developmental stages of invertebrates. Mar Ecol Prog Ser 373: 275–284.
61. Dupont S, Thorndyke MC (2009) Impact of CO_2-driven ocean acidification on invertebrates' early life-history: What we know, what we need to know and what we can do. Biogeosci Disc 6: 3109–3131.
62. Cigliano M, Gambi M, Rodolfo-Metalpa R, Patti F, Hall-Spencer J (2010) Effects of ocean acidification on invertebrate settlement at volcanic CO_2 vents. Mar Biol 157: 2489–2502.
63. Byrne M (2011) Impact of ocean warming and ocean acidification on marine invertebrate life history stages: vulnerabilities and potential for persistence in a changing ocean. Oceanogr Mar Biol Annu Rev 49: 1–42.
64. Brennand HS, Soars N, Dworjanyn SA, Davis AR, Byrne M (2010) Impact of ocean warming and ocean acidification on larval development and calcification in the sea urchin *Tripneustes gratilla*. PLoS ONE 5: e11372.
65. Talmage SC, Gobler CJ (2010) Effects of past, present, and future ocean carbon dioxide concentrations on the growth and survival of larval shellfish. Proc Natl Acad Sci U S A 107: 17246–17251.
66. Beniash E, Ivanina A, Lieb NS, Kurochkin I, Sokolova IM (2010) Elevated level of carbon dioxide affects metabolism and shell formation in oysters *Crassostrea virginica*. Mar Ecol Prog Ser 419: 95–108.
67. Vinn O, Ten Hove HA, Mutvei H, Kirsim ÄEK (2008) Ultrastructure and mineral composition of serpulid tubes (Polychaeta, Annelida). Zool J Linn Soc 154: 633–650.
68. Tanur AE, Gunari N, Sullan RMA, Kavanagh CJ, Walker GC (2009) Insights into the composition, morphology, and formation of the calcareous shell of the serpulid *Hydroides dianthus*. J Struct Biol 169: 145–160.
69. Andersson AJ, Mackenzie FT, Bates NR (2008) Life on the margin: implications of ocean acidification on Mg-calcite, high latitude and cold-water marine calcifiers. Mar Ecol Prog Ser 373: 265–273.
70. Simkiss K, Wilbur KM (1989) Biomineralization: cell biology and mineral deposition: Academic Press San Diego.
71. Allemand D, Tambutté É, Zoccola D, Tambutté S, editors (2011) Coral calcification, cells to reefs. 119–150 p.
72. Palmer AR (1992) Calcification in marine molluscs: how costly is it? Proc Natl Acad Sci U S A 89: 1379–1382.
73. Stumpp M, Dupont S, Thorndyke M, Melzner F (2011) CO_2 induced acidification impacts sea urchin larval development II: Gene expression patterns in pluteus larvae. Comp Biochem Physiol Part A 160: 320–330.
74. Li W, Gao K (2012) A marine secondary producer respires and feeds more in a high CO_2 ocean. Mar Poll Bull 64(4): 699–703
75. Melzner F, Stange P, Trübenbach K, Thomsen J, Casties I, et al. (2011) Food Supply and Seawater pCO_2 Impact Calcification and Internal Shell Dissolution in the Blue Mussel *Mytilus edulis*. PLoS ONE 6(9): e24223.
76. Cohen A, McCorkle DC, de Putron S, Gaetani GA, Rose KA (2009) Morphological and compositional changes in the skeletons of new coral recruits reared in acidified seawater: Insights into the biomineralization response to ocean acidification. . Geochem Geophys Geosyst 10(7): Q07005.
77. McClintock JB, Amsler MO, Angus RA, Challener RC, Schram JB, et al. (2011) The Mg-Calcite Composition of Antarctic Echinoderms: Important Implications for Predicting the Impacts of Ocean Acidification. J Geol 119(5): 457–466.
78. Ries JB (2004) Effect of ambient Mg/Ca ratio on Mg fractionation in calcareous marine invertebrates: A record of the oceanic Mg/Ca ratio over the Phanerozoic. Geology 32(11): 981–984.n
79. Dodd J (1967) Magnesium and strontium in calcareous skeletons: a review. J Paleontol 41(6): 1313–1329.
80. Cléroux C, Cortijo E, Anand P, Labeyrie L, Bassinot F (2008) Mg/Ca and Sr/Ca ratios in planktonic foraminifera: Proxies for upper water column temperature reconstruction. Paleoceanography 23(3): PA3214.
81. Dekens PS, Ravelo AC, McCarthy MD, Edwards CA (2008) A 5 million year comparison of Mg/Ca and alkenone paleothermometers. Geochem Geophys Geosyst 9(10): Q10001.
82. Dueñas-Bohórquez A, da Rocha RE, Kuroyanagi A, Bijma J, Reichart GJ (2009) Effect of salinity and seawater calcite saturation state on Mg and Sr incorporation in cultured planktonic foraminifera. Marine Micropaleontology 73(3–4): 178–189.

83. Allison N, Austin H, Austin W, Paterson DM (2011) Effects of seawater pH and calcification rate on test Mg/Ca and Sr/Ca in cultured individuals of the benthic, calcitic foraminifera Elphidium williamsoni. Chemical Geology 289(1–2): 171–178.
84. Heinemann A, Fietzke J, Melzner F, Bohm F, Thomsen J (2012) Conditions of Mytilus edulis extracellular body fluids and shell composition in a pH-treatment experiment: Acid-base status, trace elements and $\delta^{11}B$. Geochem Geophys Geosyst 13: Q01005.
85. Vinn O, Kupriyanova EK (2011) Evolution of a dense outer protective tube layer in serpulids (Polychaeta, Annelida). Carnets de Géologie-Notebooks on Geology CG2011_L05: 137–147.
86. Watson SA, Southgate PC, Tyler PA, Peck LS (2009) Early larval development of the Sydney rock oyster *Saccostrea glomerata* under near-future predictions of CO_2-driven ocean acidification. J Shellfish Res 28: 431–437.
87. McClintock JB, Angus RA, Mcdonald MR, Amsler CD, Catledge SA, et al. (2009) Rapid dissolution of shells of weakly calcified Antarctic benthic macroorganisms indicates high vulnerability to ocean acidification. Antarct Sci 21: 449–456.
88. Gaylord B, Hill TM, Sanford E, Lenz EA, Jacobs LA, et al. (2011) Functional impacts of ocean acidification in an ecologically critical foundation species. J Exp Biol 214: 2586–2594.
89. Feng QL, Cui FZ, Pu G, Wang RZ, Li HD (2000) Crystal orientation, toughening mechanisms and a mimic of nacre. Mater Sci Eng 11: 19–25.
90. Perez-Huerta A, Cusack M, Zhu W (2008) Assessment of crystallographic influence on material properties of calcite brachiopods. Mineralogical Magazine 72(2): 563.
91. Weiner S (2008) Biomineralization: A structural perspective. J Struct Biol 163(3): 229–234.
92. Parmigiani J, Thouless M (2006) The roles of toughness and cohesive strength on crack deflection at interfaces. J Mech Phys Solids 54(2): 266–287.
93. He MY, Bartlett A, Evans AG, Hutchinson JW (1991) Kinking Kinking of a Crack out of an Interface: Role of In-Plane Stress. J Am Ceram Soc 74 (4): 767–771.
94. Yang W, Zhang G, Liu H, Li X (2011) Microstructural characterization and hardness behavior of a biological Saxidomus purpuratus shell. Journal of Materials Science & Technology 27(2): 139–146.
95. Zhu Z, Tong H, Ren Y, Hu J (2006) Meretrix lusoria–a natural biocomposite material: In situ analysis of hierarchical fabrication and micro-hardness. Micron 37(1): 35–40.
96. Green MA, Jones ME, Boudreau CL, Moore RL, Westman BA (2004) Dissolution mortality of juvenile bivalves in coastal marine deposits. Limnol Oceanogr: 727–734.
97. Wheeler AP, Sikes CS (1984) Regulation of carbonate calcification by organic matrix. Integr Comp Biol 24: 933–944.